Ordered Meso- and Macroporous Binary and Mixed Metal Oxides

Moises A. Carreon[a,b] and Vadim V. Guliants*[a]

Keywords: Mesoporous / Macroporous / Transition metal oxides / Catalytic applications

A critical review is provided of the principles guiding the synthesis of meso- and macroporous metal oxides on multiple length scales in the presence of surfactant mesophases and colloidal arrays of monodisperse spheres, and correlations between the synthesis conditions and the properties of the resulting meso- and macroporous oxides, such as thermal stability, pore structure, elemental and nanophase compositions of the inorganic wall, etc. The thermal stability of mesostructured metal-oxide phases, in particular, is discussed in terms of charge-matching at the organic–inorganic interface, the strength of interactions between inorganic species and surfactant headgroups, the flexibility of the M–O–M bond angles in the constituent metal oxides, the Tammann temperature of the metal oxide, and the occurrence of redox reactions in the metal-oxide wall. The ordered meso- and macroporous transition-metal-oxide phases are highly promising for a range of potential applications in separations, chemical sensing, heterogeneous catalysis, microelectronics, and photonics as, respectively, insulating layers of low-dielectric-constant and photonic-bandgap materials. Furthermore, the functionalization of the internal pore surfaces in these materials and deposition of functional nanoparticles within the pores offer numerous new possibilities for molecular engineering of catalytic and other advanced nanostructured materials displaying quantum-confinement effects. The emerging catalytic applications of these novel metal-oxide phases are discussed in particular detail.

1. Introduction

Highly ordered mesoporous inorganic oxides were first reported by the researchers at Mobil Research and Development Corporation over a decade ago.[1–3] These materials, with well-defined pores up to about 3 nm in diameter, belong to the novel family of so-called M41S aluminosilicate molecular sieves[1–3] that break past the pore-size constraints of largely microporous zeotypes. Extremely high surface areas (>1000 m^2/g), finely tuned pore sizes, and flexible wall-compositions are among the many desirable properties that have made such mesoporous materials the focus of great interest for applications in heterogeneous catalysis. The preparation of the M41S phases represents a

[a] Department of Chemical and Materials Engineering, University of Cincinnati,
Cincinnati, OH 45221-0012, USA
E-Mail: Vadim.Guliants@uc.edu
[b] Current address: Materials Chemistry Research Group, Chemistry Department, University of Toronto,
80 Saint George Street, Toronto, Ontario, Canada M5S 3H6

Vadim V. Guliants was born in Baku, USSR. He studied Chemistry and obtained a Diploma with Highest Honors at Moscow State University in 1987. He received his Ph.D. in Chemistry at Princeton University in 1995 with Profs. J. B. Benziger and S. Sundaresan in the area of materials chemistry of catalytic vanadium-phosphorus oxides. After holding a research position in the area of molecular modeling, synthesis and physico-chemical characterization of crystalline microporous oxides at Praxair Inc. (Tonawanda, NY), he joined the Chemical Engineering Faculty at the University of Cincinnati in 1999. He is currently Associate Professor and Associate Head of the Department of Chemical and Materials Engineering at the University of Cincinnati. His current research is focused on the self-assembly of ordered meso- and macroporous metal oxides for applications in heterogeneous catalysis, biocatalysis and separations.

Moises A. Carreon was born in Morelia, Mexico, in 1974. He received his Bachelor's degree in Chemical Engineering at the Universidad Michoacana (UMSNH) in 1996, where he also received his Master's degree in Materials Science and Engineering in 1999. He obtained his Ph.D. degree in the Department of Chemical and Materials Engineering at the University of Cincinnati in 2003 under the supervision of Professor Vadim V. Guliants working on the hierarchical design of novel macro- and mesoporous vanadium-phosphorus-oxide phases for the selective oxidation of lower hydrocarbons. Currently he is a post-doctoral fellow in the Materials Chemistry Research Group, Chemistry Department at University of Toronto. His research centers on the molecular engineering of ordered periodic mesoporous transition metal oxides for nanotechnological applications.

MICROREVIEWS: This feature introduces the readers to the authors' research through a concise overview of the selected topic. Reference to important work from others in the field is included.

 DOI: 10.1002/ejic.200400675

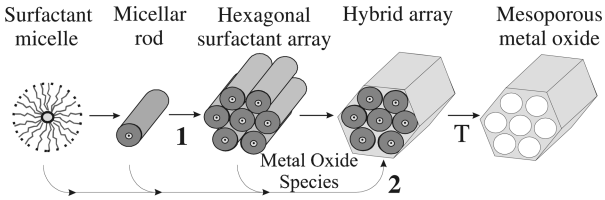

Figure 1. Self-assembly of mesoporous metal oxides possessing a 2D hexagonal pore structure.

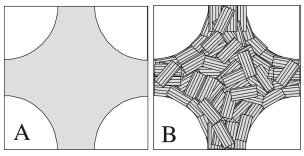

Figure 2. Mesoporous structures with (A) amorphous and (B) nanocrystalline walls.

new approach in organic-template-assisted synthesis, where, instead of individual organic molecules (as in the case of zeotypes), self-assembled molecular aggregates or supramolecular assemblies are employed as the structure-directing agents.

The discovery of M41S silicas has stimulated the search for other ordered mesostructured materials with non-silicate compositions over the last decade.[4] The general self-assembly pathway for mesostructured metal oxides is illustrated in Figure 1. Mesoporous *mixed* metal oxides are particularly promising as heterogeneous catalysts because of their tunable surface compositions, metal oxidation states (via organic-inorganic interfacial chemistry), and wall structures − amorphous or nanocrystalline (Figure 2). Furthermore, their electronic properties and the surface structure, which are critical parameters for the catalytic performance of any catalyst, are expected to change greatly in the nano regime,[5] thereby offering new, exciting possibilities for the molecular engineering of mixed metal oxides with unique catalytic, optical, and electrical properties. Ordered macroporous materials templated by ordered arrays of colloidal spheres and other shapes have recently attracted considerable attention from the scientific community.[6] The macroscale templating approach consists of the three distinct processing steps shown in Figure 3. First, the interstitial voids of the monodisperse colloidal latex sphere (approx. 100 nm to 50 μm in diameter) arrays are filled with precursors of various classes of materials, such as ceramics, semiconductors, metals, monomers, etc. In the second step, the precursors condense around the spheres and form a solid framework. Finally, the spheres are removed by either calcination or solvent extraction to form the 3D ordered macroporous structures. In this paper we critically review the current state of the art for the synthesis and emerging catalytic applications of meso- and macroporous *binary* and *mixed* metal oxides. We first discuss the structures and self-assembly mechanisms of mesoporous oxides for *silicate* compositions, since these compositions have been investigated in much greater detail than structurally similar metal oxides. We then outline synthesis guidelines for the novel

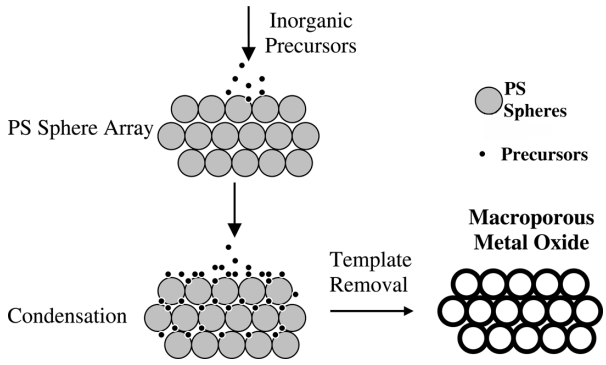

Figure 3. General procedure for the synthesis of highly ordered *macroporous* mixed-metal oxide phases employing polystyrene (PS) spheres.

mesoporous metal oxides with flexible compositions and improved thermal stability that are desirable for applications in heterogeneous catalysis. Finally, we discuss recent advances in the macroscale self-assembly of mixed metal oxides and their emerging catalytic applications.

2. Ordered Mesostructured Oxides

2.1. Structural Characteristics

Several common ordered pore-structures encountered in the M41S family are shown in Figure 4. The 2D hexagonal phase with *P6mm* symmetry, templated by hexagonal close-packed cylindrical arrays of surfactants, is the most common ordered structure. Lamellar phases are unstable upon surfactant removal, which causes the collapse of the expanded layered structures. Various cubic phases have also been reported. In the case of mesoporous silica, the bicontinuous cubic gyroid phase with *Ia3d* symmetry is found in alkali-catalyzed syntheses. This phase, with its system of interconnected pores, is much more attractive than the 2D hexagonal phase for applications requiring diffusion of species into and out of the pore network. The *Pm3n* phase templated by spherical surfactant micelles in a cubic close-packed arrangement is found in both acid- and alkaline-catalyzed syntheses of mesoporous silica.[1–3]

Figure 4. Representative members of the M41S family.

The pioneering work of Kresge et al.[1,3] and Beck et al.[2] involved only alkaline-catalyzed syntheses, and the silicates reported in their papers are referred to as MCM-41 (*P6mm*, the 2D hexagonal phase), MCM-48 (*Ia3d*, the cubic phase), and MCM-50 (the lamellar phase). The 2D hexagonal mesoporous silicas prepared by Inagaki et al.[7] from surfactant-intercalated kanemite are referred to as FSM-16. Subsequent reaction in an acidic medium led to ordered mesoporous silicas with similar pore symmetries but distinct wall properties: SBA-1 (*Pm3n*, the cubic phase), SBA-2 ($P6_3/mmc$, the 3D hexagonally packed spherical micelle phase), and SBA-3 (*P6mm*, the 2D hexagonally packed cylinders).[8] Other surfactant-templated phases include disordered materials with a wormhole network of channels, such as KIT-1[9] and MSU-1,[10] a well-defined intergrown cubic hexagonal phase STAC-1,[11] and ordered nonionic alkyl-EO_x-templated materials, for example the cubic SBA-11 (*Pm-3m*) and 3D hexagonal SBA-12 ($P6_3/mmc$).[12] Using the same methodology, triblock-copolymer-templated materials with much larger pores have also been synthesized in acidic systems, for example the 2D hexagonal (*P6mm*) SBA-15[13] and cubic cage (*Im-3m*) SBA-16 structures.[12]

Several aspects of the ordered mesoporous oxides have been reviewed by Brinker (recent advances in porous inorganic materials),[14] Vartuli et al. (synthesis of the M41S family),[15] Stucky et al. (biomimetic synthesis of mesoporous materials),[16] Raman et al. (porous silicates templated by surfactants and organosilicate precursors),[17] and Guliants et al. (mesoporous inorganic films and membranes).[18] Several synthetic strategies for the molecular design of mesoporous oxides, including those with non-siliceous compositions, have been recently reviewed by Soler-Illia et al.[19] However, thermal stability considerations for mesostructured metal oxides were not discussed in those reviews.

2.2. Self-Assembly Mechanisms And Stability Considerations

2.2.1. Liquid Crystal Templating Mechanism

A "liquid crystal templating" (LCT) mechanism of formation was proposed by the Mobil researchers, based on the similarity between liquid crystalline surfactant assemblies (i.e. lyotropic phases) and M41S.[1–3] Two mechanistic pathways were proposed to explain formation of MCM-41 containing 2D hexagonal arrays of cylindrical mesopores: 1) condensation and cross-linking of the inorganic species at the interface with a pre-existing hexagonal lyotropic liquid crystal (LC) phase, and 2) ordering of the surfactant molecules into the 2D hexagonal mesophase mediated by the inorganic species, followed by their condensation and cross-linking.

In both pathways the inorganic species, which are negatively charged at the high synthesis pH, preferentially interact with the positively charged alkylammonium headgroups of the surfactants and condense into a solid, continuous framework. The resulting organic-inorganic mesostructure could be alternatively viewed as a hexagonal array of surfactant micellar rods embedded in a silica matrix. Removal of the surfactant produces an open mesoporous MCM-41 framework. These mesophases, with pore diameters greater than 2.5 nm, generally display type IV nitrogen adsorption–desorption isotherms at 77 K, which are characteristic of mesoporous materials with an ordered, unimodal pore-size distribution. The second mechanistic pathway of LCT was proposed as a cooperative self-assembly of the alkylammonium surfactant and the silicate precursor species below the critical micelle concentration (CMC).[1–3] It is well established that no preformed LC phase is necessary for the MCM-41 formation, but, to date, the mechanistic details of the MCM-41 synthesis have not yet been fully agreed upon. Several mechanistic models have been advanced, although all share the basic idea that the silicate species promote LC phase formation below the CMC.[1–3]

2.2.2. Inorganic-Species-Driven Self-Assembly

Davis et al.[20] found that a hexagonal LC phase does not develop during the MCM-41 synthesis, based on an in situ ^{14}N NMR spectroscopic study. They proposed that, under the synthesis conditions reported by Mobil, the formation of MCM-41 begins with the deposition of two to three monolayers of silicate precursors onto isolated surfactant micellar rods. The silicate-encapsulated rods are randomly ordered, and eventually pack into a hexagonal mesostructure. Heating and aging completes the condensation of the silicates into the obtained MCM-41 mesostructure.

Steel et al.[21] postulated that surfactant molecules assemble directly into the hexagonal LC phase upon addition of the silicate species, based on their ^{14}N NMR spectroscopic data. The silicates organize into layers, with rows of cylindrical rods intercalated between the layers. Aging the mixture causes the layers to pucker and collapse around the rods, which then transform into the surfactant-containing 2D hexagonal MCM-41 structure.

The "charge density matching" mechanistic model proposed by Monnier et al.[22] and Stucky et al.[23] suggests that MCM-41 could be derived from a lamellar phase. The initial phase of the synthesis mixture is layered, as detected by X-ray diffractometry (XRD), due to the electrostatic attraction between the anionic silicates and the cationic surfactant head-groups. As the silicate species begin to condense, the charge density is reduced. Accompanying this process, a curvature is introduced into the layers to maintain the charge-density balance with the surfactant headgroups, which transforms the lamellar phase into a hexagonal mesostructure.

Under synthesis conditions that prevent condensation of the silicate species, such as low temperatures and high pH (ca. 14), a truly cooperative self-assembly of the silicates and surfactants was found to be possible. Firouzi et al.[24] showed, through ^{2}H and ^{29}Si NMR spectroscopy and neutron scattering, that a micellar solution of CTAB (cetyltrimethylammonium bromide) transforms into a hexagonal phase in the presence of silicate anions. This is consistent with the effect of electrolytes on micellar phase-transi-

tions.[25] The silicate anions ion-exchange with the surfactant halide counterions to form a "silicatropic liquid crystal" (SLC) phase that involves silicate-encrusted cylindrical micelles. This SLC phase exhibited behavior very similar to typical lyotropic systems, except that the surfactant concentrations were much lower and the silicate counterions were reactive.[26] Heating the SLC phase caused the silicates to condense irreversibly into MCM-41. Firouzi et al.[24,26] also demonstrated that, in addition to the charge-balance requirement (i.e. electrostatic interaction), there was preferential bonding of the alkylammonium head-groups to multi-charged D4R (double four-ring, $[Si_8O_{20}]^{8-}$) silicate anions under the high pH conditions.

All these previous theories have regarded the formation of MCM-41 as a series of events that occur homogeneously throughout an aqueous solution. Recent work has shown, however, that MCM-41 might be formed heterogeneously. Regev,[27] for example, has found evidence for MCM-41 intermediate structures in the form of clusters of rod-like micelles "wrapped" by a coating of silicate from low-temperature transmission electron microscopy (TEM) and small-angle X-ray scattering. These clusters of elongated micelles were found before precipitation occurred. According to Regev,[27] as the reaction progresses, the silicate species diffuse to, and deposit on, the individual surfaces of the micelles within the cluster. The clusters of elongated micelles therefore eventually become clusters of silicate-covered micelles. Thus, the clusters of micelles serve as nucleation sites for MCM-41 formation.

Frasch et al. have proposed a modified mechanism for the formation of 2D hexagonal silica.[28] The silicate–counterion exchange at the micellar surface was followed by fluorescence techniques using pyrene or dipyrenylpropane as fluorescent probes. The variation of the properties of CTAB and CTACl (cetyltrimethylammonium chloride) micelles upon the successive addition of a large excess of base [NaOH or TMAOH (tetramethylammonium hydroxide)] and silicate species was studied. Their results showed that, prior to the formation of the ordered mesophase, the interactions between the silicate species and surfactant micelles are weak. They therefore proposed a new model for the formation of mesostructured silica in which the key step is the formation of siliceous pre-polymers. According to this model, the growing pre-polymers interact with an increasing number of surfactant molecules to form hybrid silica-surfactant micellar aggregates. Further polymerization of these complexes takes place during the precipitation/aging process to give ordered mesostructured silica. The formation of mesoscopically ordered silica/surfactant composites under acidic synthesis conditions was studied by time-resolved in situ small-angle X-ray scattering (SAXS) using synchrotron radiation.[29] The various proposed mechanisms of formation of ordered mesostructured phases have been recently reviewed by Zana et al.[30] Recently, Linden et al.[31] have followed the initial stages of the formation of SBA-15 by in situ SAXS/XRD using synchrotron radiation. The authors proposed that the first step in the formation of an SBA-15 mesostructure is the liquid–liquid phase separation of spherical P123-silicate hybrid micelles; nucleation and growth of the 2D hexagonal phase then takes place.

2.3. Thermal Stability of Mesostructured Phases

The high thermal stability of mesostructured phases is perhaps the most critical requirement for their applications in heterogeneous catalysis. In general, the thermal stability of mesostructured metal-oxide phases depends on: (1) the degree of charge-matching at the organic–inorganic interface, (2) the strength of interactions between inorganic species and surfactant head-groups, (3) the flexibility of the M–O–M bond angles in the constituent metal oxides, (4) the Tammann temperature of the metal oxide, and (5) the occurrence of redox reactions in the metal-oxide wall.

The *charge-matching* at the organic–inorganic interface enables control over the wall composition and facilitates cross-linking of the inorganic species into a robust mesostructured network. A knowledge of the electrokinetic behavior (i.e. the isoelectric points) of the inorganic species in solution is required for fine-tuning electrostatic and other interactions at the inorganic–organic interface in order to obtain thermally stable mesoporous phases.[32] The isoelectric points of common transition-metal solid oxides and hydroxides are shown in Table 1.[32,33] The presence of strong *covalent bonds* between metal-oxide species and surfactant head-groups, for example metal–N bonds, means that harsh conditions, such as combustion, are required for surfactant

Table 1. Isoelectric points of common transition metal oxides.[28,29]

Metal oxide	Isoelectric point	General comments
V_2O_5	0.5	oxovanadium(v) species
MoO_3	<0.5	NA
Nb_2O_5	<0.5	NA
TiO_2	4.7	natural rutile
TiO_2	6.2	synthetic rutile, anatase
ZrO_2	4.0	natural mineral
ZrO_2	6.7	$Zr(NO_3)_4$ + NaOH
Y_2O_3 (hydrous)	8.95	$Y(NO_3)_3$ + NaOH
NiO	10.3 ± 0.4	NiO
WO_3 (hydrous)	0.5	Na_2WO_4 + HCl
MgO	12.4 ± 0.3	MgO
MnO_2	4.0–4.5	$Mn(NO_3)_2$ + HCl
α-Fe_2O_3	8.7	hydrolysis of $Fe(NO_3)_3$ solution
γ-Fe_2O_3	6.7 ± 0.2	precipitation of FeOOH
Fe_3O_4	6.5 ± 0.2	natural magnetite

Table 2. Tammann temperatures of some common transition-metal oxides.[5,34]

Metal oxide	M. p. (K)	Tammann temp. (K)
V_2O_5	943	472
MoO_3	1068	534
Nb_2O_5	1784	892
TiO_2	2128	1064
ZrO_2	2983	1492
NiO	2257	1129
WO_3	1745	873
MgO	3125	1563
MnO	1923	962
Fe_2O_3	1838	919

removal, and these may lead to collapse of the mesostructure. Similarly, *rigid M–O–M bond angles* that are unable to accommodate the curvature of the inorganic–organic interface may result in the formation of only lamellar or dense metal-oxide phases. On the other hand, metal-oxide species should possess low lattice mobility at elevated temperatures in order to prevent transformation of the mesostructured metal oxides into more thermodynamically stable dense phases. The mobility of metal ions or atoms in a crystalline metal oxide increases rapidly in the vicinity of its *Tammann temperature*, defined as $0.5–0.52T_m$, where T_m is the melting point in Kelvin.[34] Therefore, it is not surprising that the low Tamman temperature of some transition- metal oxides[5,35] translates into a limited thermal stability of the corresponding mesostructures (Table 2). Finally, the structural collapse of mesophases may be caused by *redox reac-*

Table 3. Mesostructured and mesoporous *binary* metal oxides.

Framework composition	Precursors	Mesophase and unit cell parameter (Å)	Ref.
Vanadium oxide[c]	ammonium vanadate, CTACl, H_2O	lamellar (c = 27) hexagonal (a = 39)	[56]
Vanadium oxide[a]	V_2O_5, DTABr, H_2O	lamellar (c = 21.6)	[57]
Vanadium oxide[a]	oxovanadium triisopropoxide, dodecylamine, ethanol/H_2O	lamellar (c = 23–28) hexagonal (a = 34.6)	[58]
Vanadium oxide[a]	VCl_4, triblock copolymers, ethanol	mesostructured (lack of long-range order) (maximum d-spacing 111)	[59]
Vanadium oxide[c]	$VOSO_4$, P123, ethanol/H_2O	wormhole like (channel spacing 30–40)	[60]
Molybdenum oxide[a]	Na_2MoO_4, H_2MoO_4, DTABr, H_2O	lamellar (c = 22.9)	[57]
Molybdenum oxide[a]	$MoCl_5$, triblock copolymers, ethanol	mesostructured (lack of long-range order) (maximum d-spacing 100)	[59]
Niobium oxide[b]	niobium ethoxide, sodium dodecyl sulfate, sodium dodecyl phosphonate, primary alkylamines	lamellar (c = 25) hexagonal (a = 32–52), cubic (d-spacing 48)	[61,62]
Niobium oxide[b]	$NbCl_5$, tribolck copolymers, ethanol	hexagonal (a = 32–52)	[59,63]
Titanium oxide[b]	$TiCl_4$, triblock copolymers, ethanol	hexagonal (a = 117) cubic (a = 107)	[59,63]
Titanium oxide[c]	peroxytitanates, CTACl, H_2O	lamellar (c = 31) hexagonal (d-spacing 41)	[69]
Titanium oxide[a]	titanium isopropoxide, CTABr, ethylene glycol, NaOH,	mesostructured (lack of long-range order) (channel spacings 50)	[70]
Zirconium oxide[b]	zirconium n-propoxide, H_2O, carboxylates, alkyl sulfonates, dodecyl sulfate, primary alkylamines	lamellar, hexagonal, mesostructured (lack of long-range order) (maximum d-spacings = 16–40)	[80]
Zirconium oxide[b]	$ZrCl_4$, triblock copolymers, ethanol	hexagonal (a = 122)	[59,63]
Zirconium oxide[a]	$Zr(OC_2H_5)_4$, CTABr, ethylene glycol, NaOH	mesostructured (lack of long-range order) (channel spacings = 31–37)	[70]
Hafnium oxide[b]	$HfCl_4$, H_2O, CTABr	wormhole-like (channel spacings 40)	[82]
Hafnium oxide[b]	$HfCl_4$, triblock copolymers, ethanol	mesostructured (lack of long-range order) (maximum d-spacing 124)	[59,63]
Tantalum oxide[b]	tantalum ethoxide, octadecylamine, H_2O	hexagonal (a = 33–50)	[86]
Tantalum oxide[b]	$TaCl_5$, triblock copolymers, ethanol	hexagonal (a = 78)	[59,63]
Nickel oxide[a]	$NiSO_4$ $6H_2O$, CTABr, H_2O	disoredered + lamellar (channel spacings = 46)	[89]
Yttrium oxide[a]	$Y(NO_3)_3$ $6H_2O$, dodecylsulfate, H_2O, urea	lamellar (c = 40), hexagonal (a = 62)	[91]
Rhenium oxide[a]	methyltrioxo-rhenium, primary alkylamines, H_2O	disordered + lamellar (channel spacings = 25–33)	[92]
Manganese oxide[c]	$MnCl_2$ $4H_2O$, H_2O, $C_{12}H_{25}NMe_3OH$	lamellar, disordered (d-spacing 42)	[90]
Tungsten oxide[a]	H_2WO_4, DTABr, H_2O	Keggin-type structure	[57]
Tungsten oxide[b]	WCl_6, triblock-copolymers, ethanol	mesostructured (lack of long-range order) (maximum d-spacing 126)	[59,63]
Iron oxide	iron(III) ethoxide, CTAB	mesoporous and lamellar	[96,97]

[a] Thermally unstable. [b] Thermally stable. [c] Partially stable (up to 625 K) or after solvent extraction.

tions occurring in the metal-oxide wall during surfactant removal or catalytic reaction.

Accordingly, we review below the synthesis, pore structures, elemental and nanophase compositions, thermal stability, and emerging applications of mesoporous metal oxides in heterogeneous catalysis.

2.4. Binary Mesostructured Metal Oxides

The mesostructured binary transition metal oxides that are promising for applications in heterogeneous catalysis are summarized in Table 3. High-resolution TEM images of the three most-common porous structures observed in mesostructured metal oxides − lamellar, hexagonal, and cubic − are illustrated in Figure 5, Figure 6 and Figure 7, respectively. Metal oxides containing 2D hexagonal and cubic mesopore structures are characterized by the unimodal pore-size distributions and type IV adsorption–desorption isotherms typical of mesoporous materials (Figure 8).

Vanadium-, molybdenum-, and niobium-based mixed metal oxides are particularly promising as catalysts or catalytic supports for selective oxidation reactions.[36–50] For example, supported vanadium oxide catalysts are widely used for the partial oxidation of olefins,[51] aromatics,[52] and methanol,[53] the selective catalytic reduction of NO_x,[54] and ammoxidation of aromatics.[55] Molybdenum- and niobium-based oxides are catalytically active in the selective oxidation and reduction of hydrocarbons.[39] Mesostructured vanadium oxide was reported for the first time by Luca et al.[56] They suggested that anionic vanadate species self-assemble with the cationic head-group of cetyltrialkylammonium chloride surfactant (CTACl) in alcoholic media to produce the mesostructure. Although the structural order was retained after low-temperature calcination, both porosity studies and thermogravimetric analysis indicated that the surfactant was only partially removed, thus leading to thermally unstable phases. Other attempts to prepare mesoporous vanadium oxide have been reported. Whittingham et al.[57] have prepared a mesostructured, layered vanadium oxide by hydrothermal treatment of V_2O_5 in the presence of dodecyltrimethylammonium bromide (DTAB). However, the DTAB surfactant was not removed upon cation exchange. Sayari et al.[58] have synthesized lamellar and hexagonal mesostructured vanadium oxide by hydrolyzing oxovanadium triisopropoxide in the presence of dodecylamine, although no attempt was made to remove the surfactant. A mesostructured vanadium oxide obtained from the assembly of triblock copolymers with VCl_4 has been re-

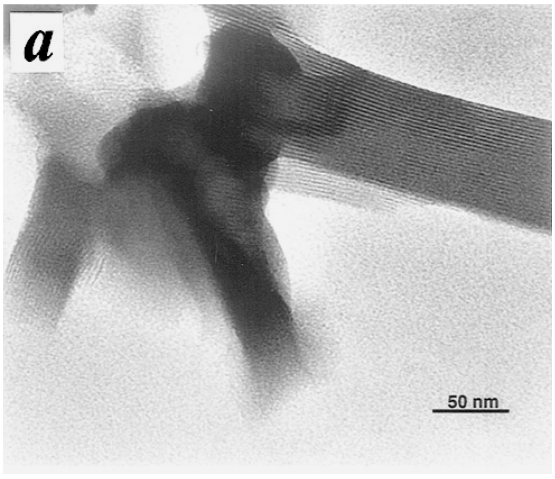

Figure 5. TEM of *lamellar* mesostructured vanadium oxide.[58]

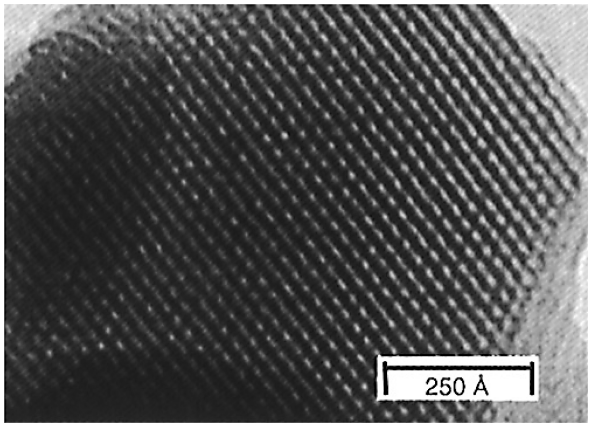

Figure 6. TEM of *hexagonal* mesoporous niobium oxide.[61]

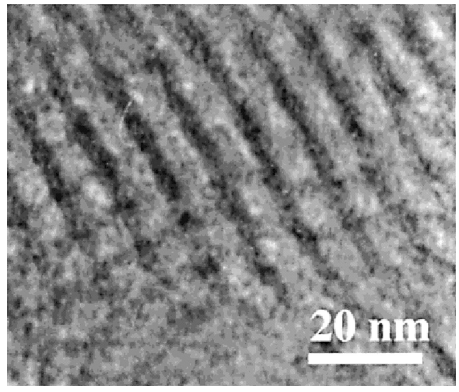

Figure 7. TEM image of *cubic* mesoporous zirconium oxide.[59]

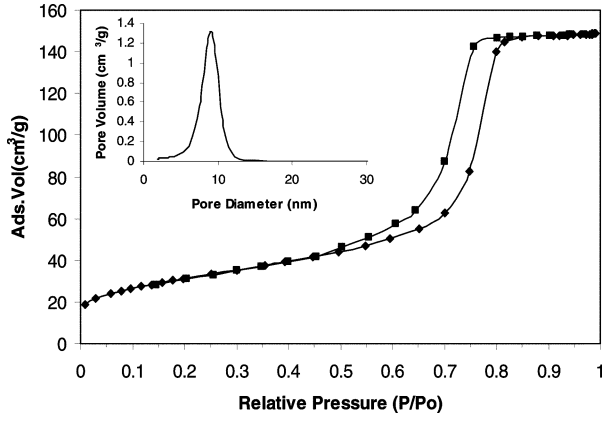

Figure 8. Nitrogen adsorption–desorption isotherms and BJH pore-size distribution plot (inset) for mesoporous niobium.

ported by Stucky et al.,[59] although it lost its mesoscopic order upon calcination. Liu et al.[60] have reported the synthesis of mesostructured V_2O_5 by electrochemical deposition using nonionic surfactants. The final wormhole mesostructure was found to contain 3–4 nm pores. Although the complete removal of the surfactant was reported by the authors, no surface area or pore data were provided. The low Tammann temperature of V_2O_5 (472 K), as well as the cycles of redox reactions during surfactant combustion, account for the poor thermal stability of this oxide system.

Mesostructured molybdenum oxides have also been reported by Whittingham et al.[57] and Stucky et al.[59] A layered structure with a repetitive interplanar distance of 22 Å was prepared by hydrothermal reaction of molybdic acid with DTAB.[57] A mesostructured molybdenum oxide with larger ordering lengths (100 Å) was successfully synthesized by the assembly of triblock copolymers with $MoCl_5$. However, the obtained mesostructured materials were unstable upon calcination.[57,59] Incomplete condensation of the inorganic frameworks, the cycles of redox reactions during surfactant combustion, as well as the low Tammann temperature of the constituent metal oxides, are mainly responsible for the poor thermal stability of these metal-oxide mesophases. On the other hand, thermally stable mesoporous Nb_2O_5 has been obtained by Ying et al.[61,62] in the presence of amines as structure-directing agents. They proposed a ligand-assisted liquid-templating mechanism for the formation of thermally stable mesoporous Nb and Ta oxides. The formation of covalent bonds between Nb and the N-atom of the amine template directs the interaction between the organic and inorganic species. The improved thermal stability of mesoporous niobium oxide is probably due to the relatively high Tammann temperature of niobium oxide (892 K). High specific surface areas (approx. 600 m^2/g) were observed for these mesophases after template removal by acid/solvent extraction with triflic acid. In a different approach, Stucky et al.[59,63] have prepared mesoporous niobium oxide with pores of about 50 Å and a surface area of about 190 m^2/g using triblock copolymers as structure-directing agents. The improved thermal stability of these phases was attributed to weak H-bonding interactions between the template and inorganic walls, making the template removal possible without damaging the inorganic framework.

Titania possesses very interesting catalytic, photochemical, and electrical properties, which make it an attractive system for several applications. For instance, TiO_2 is commonly used as a photocatalyst.[64,65] Crystalline titania modified with sulfate ions is an active catalyst for low-temperature esterification, isomerization, alkylation, and cracking of hydrocarbons.[66,67] Other applications of titania are as an electrode material in electrochemistry, a capacitor in electronics, in humidity and gas sensors, and in photovoltaic solar cells.[68]

Mesoporous TiO_2 has been obtained using different synthetic approaches.[59,63,69,70] Stucky et al.[59,63] have employed hydrogen bonding to direct the synthesis and obtained large-pore (ca. 65 Å) hexagonal and cubic mesoporous TiO_2 with a specific surface area of 200 m^2/g. Interestingly, the walls of the TiO_2 mesostructure were built of nanocrystalline anatase, which is promising for potential applications in photocatalysis, since anatase is the most photocatalytically active crystalline phase of TiO_2.[65] In a different approach, charge matching between cationic surfactants and anionic peroxytitanates was used to produce mesoporous TiO_2 [69] with a surface area of 310 m^2/g and a pore size of about 36 Å. The final mesostructure, however, was found to lack long-range order, thus suggesting the formation of a wormhole pore network. A nonaqueous route for the preparation of mesostructured titania was studied by Kuperman et al.[70] The final mesoporous structures, with surface areas of up to 420 m^2/g, were thermally stable only when silanol groups were incorporated into the inorganic framework by the gradual exposure of the inorganic framework to 7–15 wt.-% of Si_2H_6. The composite was then heated to 125 °C and the excess of unreacted Si_2H_6 was removed under vacuum.

Zirconium oxide is a particularly interesting catalytic system, and has found many uses in chemical and petrochemical processes because it possesses acidic, basic, and redox properties. For example, it is an effective catalyst for the selective formation of isobutane and isobutene from synthesis gas,[71,72] and acts as a superacid (sulfated ZrO_2) in the isomerization and cracking of paraffins and alkylation and acylation of aromatics.[73–76] Crystalline *stable* tetragonal or cubic zirconia is required in most catalytic applications. For example, the tetragonal ZrO_2 phase has been claimed as the active phase in *n*-butane isomerization[76,77] and alkylation and acylation of aromatic compounds.[78,79]

Wong and Ying[80] have studied the formation of mesostructured ZrO_2 directed by anionic and nonionic surfactants. High-surface-area (360 m^2/g), mesoporous ZrO_2 was obtained only when alkyl phosphate surfactants were used. They associated the enhanced thermal stability of the final mesoporous structure with the presence of the phosphate groups on the ZrO_2 surface after the surfactant removal. However, no specific details were provided for the role of phosphate in stabilizing the ZrO_2 mesostructure.

Other mesoporous zirconia with pore sizes between 58 and 62 Å[59,63] and wormlike zirconia[70] have been also reported. For instance, thermally stable mesoporous zirconia with a surface area of about 280 m^2/g has been prepared,[59] although the mesostructure was only stable when SiO_2 was incorporated into the zirconia wall during synthesis. Mesoporous zirconia with both amorphous[70] and tetragonal nanocrystalline[59,63] walls has also been prepared, thus allowing an exploration of the role of the extended crystal structure on the catalytic properties of this metal oxide.

Sulfated hafnium oxide is another attractive superacid system for selective alkane isomerization.[81] The thermally stable hafnium oxide reported by Sayari et al.[82] exhibits a high surface area (ca. 200 m^2/g) and a wormhole pore-structure without long-range structural order. The pore diameter evaluated by the Horvath–Kawazoe method was only 11 Å, thus indicating the formation of a microporous phase. Mesoporous HfO_2 with large pores (70 Å) has also been

prepared by a neutral self-assembly approach employing Pluronic P-123 as a structure-directing agent.[59,63]

Tantalum oxide is yet another interesting metal-oxide system with potential applications in photocatalysis, such as photocatalytic water splitting.[83–85] Hexagonal mesoporous Ta_2O_5 with pore sizes in the 20–40 Å range and specific surface areas of up to 500 m^2/g was reported for the first time by Antonelli and Ying.[86] The synthesis was directed by covalent bonding between the primary alkylamine headgroups and Ta atoms in a ligand-assisted liquid-templating mechanism. Similar to the synthesis of mesoporous Nb_2O_5, mesoporous Ta_2O_5 has also been obtained in the presence of nonionic surfactants (Pluronic P-123) by neutral self-assembly directed by hydrogen-bonding interactions.[59,63]

Other reported mesostructured binary oxides with potential applications in catalysis are NiO and MnO_2. Nickel-oxide-based catalysts have been used successfully in the partial oxidation of olefins, nitroxidation of hydrocarbons into nitriles, and partial oxidation of isobutylene into methylacrolein.[87] Manganese oxides show catalytic activity in the oxidation of alkanes.[88] Shih et al.[89] have investigated the synthesis of mesostructured nickel oxide in the presence of CTAB. The NiO mesostructure was thermally unstable and collapsed upon thermal treatment. Since NiO exhibits a high Tammann temperature (1129 K), the limited stability of this mesostructured oxide may be associated with a low degree of cross-linking, redox reactions, and rigidity of the Ni–O–Ni framework. However, the addition of sodium silicate during the NiO synthesis produced a thermally stable mesostructure with a surface area of 530 m^2/g. The addition of silicate (Si/Ni = 0.2–0.5) is believed to strengthen the inorganic mesostructure. It was suggested that the resultant mesophase had a structure of SiO_4 tetrahedra linked together by Ni atoms on every corner to produce a robust mesostructure. Mesostructured lamellar manganese oxide has been prepared by Suib et al.[90] by employing $(C_{12}H_{25})NMe_3OH$ as a surfactant. However, no information was provided on the surfactant removal from these lamellar manganese oxides.

Other reported mesostructured transition-metal oxides include Y_2O_3, WO_3, and ReO_2: yttrium oxide is used as a matrix for solid-state lasers and luminescent systems,[91] rhenium oxides exhibit interesting electrical conductivity properties,[92] while tungsten oxides have found applications as semiconductor materials.[59,63] Lamellar and hexagonal mesostructured yttrium oxides have been prepared by employing anionic surfactants, such as sodium dodecylsulfate.[91] In this case, removal of the surfactant led to high surface areas (ca. 550 m^2/g) and mesoporous structures with pores of about 30 Å. Mesostructured rhenium oxide exhibiting wormhole channels occupied by surfactant molecules has been prepared employing dodecylamine as a surfactant.[92] However, no porosity was observed after the surfactant removal, indicating that the mesostructure collapses under oxidizing conditions, while the pores were blocked with residual pyrolyzed carbon after a thermal treatment in an inert atmosphere. Mesostructured tungsten oxide has been prepared in the presence of DTAB; however, DTAB removal by cation exchange was not successful.[57] High surface area WO_3 (125 m^2/g) displaying pores of about 50 Å has also been prepared by employing Pluronic P-123 as a structure-directing agent.[59,63]

Iron oxide is another interesting catalytic system that has been used to catalyze the oxidative dehydrogenation of hydrocarbons. For example, hematite is an active catalyst for transforming butane[93,94] and ethylbenzene.[95] High-surface-area (274 m^2/g) mesoporous iron oxides have been synthesized by sonochemical synthesis.[96,97] Iron(III) ethoxide was used as the inorganic precursor and CTAB as surfactant. Since the self-assembly process is directed by strong coulombic interactions, the improved thermal stability of mesostructured iron oxide may be associated with its relatively high Tamman temperature (919 K).

In addition to the above-mentioned applications in catalysis, these metal oxides (Table 3) may also be used as mesoporous hosts for the growth of functional nanoparticles, such as supported metals for applications in catalysis and semiconductor nanoparticles for electronic and optical applications.[98–100]

2.5. Mesostructured Mixed-Metal Oxides

Mixed-metal oxides are particularly attractive as catalysts for the selective oxidation of lower alkanes. For example, vanadium-phosphorus oxides are highly active and selective for the oxidation of *n*-butane to maleic anhydride.[101–105] The recently reported bulk mixed Mo-V-Sb-Nb oxides[101–104] are active and selective for the oxidation of propane to acrylic acid, and it is well known that the most efficient catalysts for propane ammoxidation are based on bulk mixed-metal oxides (i.e. vanadium antimonates or promoted molybdates).[110,111] V-Mg oxides are very active in the oxidative dehydrogenation of light alkanes to alkenes.[112,113] Mesostructuring of these complex metal-oxide systems offers the possibility to design novel catalytic materials with high surface areas, controlled porosities, tunable surface compositions, and improved catalytic performance. Examples of mesostructured mixed-metal oxides most relevant to applications in catalysis are summarized in Table 4.

One of the most remarkable mixed-metal oxide systems is the vanadium-phosphorus-oxide (VPO) system for the oxidation of *n*-butane to maleic anhydride, which is the only industrial vapor-phase oxidation of an alkane.[101–105] Few reports exist on the synthesis of mesostructured VPO materials. Iwamoto et al.[114] have reported the synthesis of mesostructured hexagonal vanadium-phosphorus oxide materials using alkyltrimethylammonium surfactants (C_{12}–C_{16}). However, the mesostructure in these materials was lost upon calcination. Doi and Miyake[115] have reported the synthesis of a novel hexagonal mesostructured VPO compound from the VPO catalyst precursor $VOHPO_4 \cdot 0.5H_2O$ by surfactant intercalation and subsequent hydrothermal treatment. However, these materials suffer from poor thermal stability and low phosphorus content that are detri-

Table 4. Mesostructured and mesoporous *mixed* metal oxides.

Framework composition	Precursors	Mesophase and unit cell parameter (Å)	Ref.
VPO[a]	$VOSO_4$, H_3PO_4, C_nTACl, H_2O, n = 12,14,16	hexagonal (maximum d-spacing 33–40)	[114]
VPO[a]	$VOHPO_4$ 0.5 H_2O, C_{14}TAMCl, H_2O	lamellar (channel spacing 30) and hexagonal (NA)	[115]
VPO[a]	V_2O_5, H_3PO_4, CTABr, H_2O, V metal	hexagonal (ICMUV-2) (a = 42–46)	[116]
VPO[a]	V_2O_5, H_3PO_4, CTAOH, CTACl, H_2O, V metal	lamellar (c = 32.2), hexagonal (a = 50.5), cubic (a = 85.4)	[117]
VPO[a]	$VOSO_4$, $VO(acac)_2$, H_3PO_3, H_3PO_4, H_2O, alkylamines, sulfonates, phosphonates, alkyltrimethylammonium bromide	lamellar (c = 23–32), hexagonal (a = 40–44), cubic (a = 92–99)	[118–121]
Nb-Ta oxide[b]	$NbCl_5$, $TaCl_5$, P123, MeOH, EtOH, ButOH, HexOH	disordered mesoporous structure (channel spacings 30–40)	[122]
Nb-V oxide[b]	vanadium triisopropoxy oxide, niobium ethoxide, octadecylamine, ethanol/H_2O	wormhole pore structure (maximum d-spacing 40)	[123]
Mg-V oxide[b]	$V(acac)_3$, $MgCl_2$, DTABr, MTABr, CPBr, CTABr, SDS, SDBS, BTABr, H_2O	lamellar (c = 35), wormlike channel spacing 38), hexagonal (a = 36)	[112,113]
TiO_2-PO_4 [b]	titanium methoxide, H_3PO_4, dodecanol + 5 EO tenside, H_2O	disordered hexagonal (maximum d-spacing 62)	[124]
TiO_2-PO_4 [b]	titanium propoxide, H_3PO_4, H_2O $CH_3(CH_2)_n$ $N(CH_3)_3Br$, n = 7,11,15,17,	hexagonal (a = 33–55) lamellar	[125]
TiO_2-PO_4 [b]	titanium isopropoxide, H_3PO_4, C $_n$ TABr (n = 16, 18, 20), H_2O	hexagonal (d-spacing 27–36)	[126]
ZrO_2-SO_4, ZrO_2-PO_4 [b]	zirconium propoxide, ammonium sulfate, H_3PO_4, CTABr, OTABr, H_2O	hexagonal (a = 30–51)	[127]
Y_2O_3-ZrO_2 [b]	zirconium ethoxide, ethylene glycol, yttrium acetate, CTABr, H_2O	wormhole (d-spacings 42–46)	[138]
Y_2O_3-ZrO_2 [a]	$ZrO(NO_3)_2$, Y_2O_3, SDS, urea, H_2O	lamellar (c = 32–35) and hexagonal (a = 44)	[139]
Zr-Ti oxide[b]	$ZrCl_4$/$TiCl_4$, triblock copolymers, ethanol	NA (d-spacing 103)	[59,63]
Zr-W oxide[b]	$ZrCl_4$/WCl_4, triblock copolymers, ethanol	NA (d-spacing 100)	[59,63]

[a] Thermally unstable. [b] Thermally stable.

mental for their use as heterogeneous catalysts. Amoros et al.[116] have described the synthesis of hexagonal mesostructured oxovanadium phosphates, denoted as ICMUV-2. However, the removal of surfactant from their vanadium phosphates resulted in the collapse of the mesostructure. Mizuno et al.[117] have described the synthesis of hexagonal, cubic, and lamellar mesostructured vanadium-phosphorus-oxides that lose their structural order upon calcination. We recently reported novel hexagonal, cubic, and lamellar VPO phases, which displayed improved thermal stability, desirable chemistries (i.e. the P/V ratios and vanadium oxidation states), and pore structures for the partial oxidation of lower alkanes.[118–120] We demonstrated in these studies that the V oxidation state and the surface P/V ratios can be tuned, respectively, by post-synthesis thermal treatment (i.e., oxidizing vs. reducing atmosphere) and inorganic–organic interfacial chemistry (i.e., the surfactant functionality).[118,121] The N_2 adsorption–desorption isotherm measurements indicated that these novel VPO phases have a broad size-distribution in the micropore range. However, complete removal of the surfactant and achievement of thermal stability for the mesoporous VPO system still represents a major challenge.[121] The incomplete cross-linking of the VPO framework, its redox properties, and the low Tammann temperature of the constituent oxides have so far prevented the preparation of thermally stable mesoporous VPO phases.

The Nb and Ta oxides possess moderately strong Lewis and Brønsted acidity and are promising as solid-acid catalysts and catalytic supports.[50] The mesoporous mixed Nb/Ta (ca. 1:1) oxide displaying a wormhole pore structure was prepared by a neutral templating method.[122] Interestingly, the resultant mesostructure displayed not only high thermal stability, but also the presence of nanocrystalline walls. However, as the crystallinity of the mesostructure increased with calcination time, the BET surface areas decreased from 168 to 22 m^2/g, suggesting the densification of the final mesostructure. In order to prevent this decrease in surface area, Antonelli et al.[123] have employed the ligand-assisted method to prepare mesoporous V-Nb oxides (5–15 mol.-% V in mesoporous niobium oxide). Although high-surface-area composites (500–830 m^2/g) were reported, only disordered wormhole pore structures were obtained, with walls about 2.0–2.3 nm thick. Chao and Ruckenstein have succeeded in the preparation of mesoporous Mg-V oxides (Mg/V = 0.5–10) with relatively high surface areas (i.e. 70–250 m^2/g) and wormhole-like pores that are promising for the oxidative dehydrogenation of alkanes.[112–113] The pore size of these composites could be fine-tuned by changing the pH. They proposed a self-assembly mechanism in which anionic polyvanadate species associated with an Mg^{2+} cation condense around positively charged surfactant micelles. The thermal stability of this system was attributed to the incorporation of Mg cations into the inorganic oxovanadium

framework. Figure 9 shows the typical wormhole-like mesoporous structure of mixed transition-metal oxides.

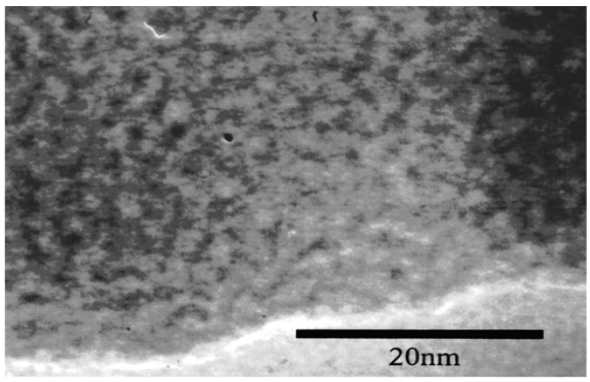

Figure 9. TEM of mesostructured vanadium-magnesium oxide exhibiting wormhole channels occupied by surfactant molecules.[112]

Mesoporous titanium phosphate is another example of a mixed-metal oxide obtained by a templated self-assembly approach.[124–126] Crystalline phosphated titania is catalytically active in the isomerization and alkylation of hydrocarbons.[66–67] Mesoporous titanium phosphate was prepared by a neutral templating route employing poly(ethylene oxide)s as surfactants.[124] The final mesostructure displayed thermal stability and high surface area (≈ 350 m^2/g). The relatively high thermal stability of mesoporous titanium phosphate was associated with a high degree of condensation of the amorphous titanium phosphate framework, which prevents crystallization and densification of the mesostructure. However, the obtained mesostructures were highly disordered, suggesting that weak hydrogen-bonding interactions between the surfactant and inorganic species lead to a decrease in the structural order. The synthesis of mesoporous phosphated titania (P/Ti = 1 and 2) has also been directed by electrostatic interactions.[125] In this case, disordered mesostructures with much higher surface areas (up to 740 m^2/g) and wormhole-like pores were obtained after surfactant extraction. However, the surface area decreased by about 60 % upon calcination. Titanium phosphates possessing ordered hexagonal mesostructure have been obtained by Schüth et al. in the presence of alkyltrimethylammonium bromides.[126] Interestingly, the pore analysis showed a type-I isotherm that is characteristic of microporous materials after surfactant removal by calcination, which suggests the formation of a hierarchical porous structure in which the micropores are most likely incorporated in the walls of the mesostructure.

Low-temperature alkane isomerization is of great interest to the petrochemical industry since branched alkanes are important gasoline products and additives.[104] Superacids, such as ZrO_2-SO_4 and ZrO_2-PO_4, catalyze alkane isomerization and other reactions demanding high acidity.[73–75] Highly ordered and thermally stable hexagonal mesoporous ZrO_2-SO_4 and ZrO_2-PO_4 have been reported by Schüth et al.[127] In these studies, the improved thermal stability was associated with the presence of the sulfate and phosphate groups, which strengthen the walls of ZrO_2. The authors proposed that uncondensed ZrOH groups bond with phosphate groups, thereby increasing the extent of cross-linking and enhancing the stability of the mesophase upon surfactant removal.

Mixed yttrium-zirconium oxide is an example of a catalytic system that is promising for the Fischer–Tropsch synthesis.[128] Yttria is commonly used to stabilize the tetragonal or cubic ZrO_2 phase.[129,130] When Y is incorporated into the ZrO_2 lattice, oxygen vacancies are created to preserve the lattice neutrality. It has been suggested that the active sites for CO hydrogenation are these oxygen vacancies.[128] Mesoporous yttria-zirconia with nanocrystalline walls, wormhole pore channels of about 20 Å, and 100–250 m^2/g BET surface areas has been reported by Ozin et al.,[131] whereas Gedanken et al.[132] have prepared lamellar and hexagonal Y/Zr (1:1) oxide mesostructures by a sonochemical method employing sodium dodecyl sulfate as the surfactant. Mesoporous structures with surface areas of about 245 m^2/g were obtained after surfactant extraction with sodium acetate. However, a nonuniform pore-size distribution was observed, and the mesoporous mixed-metal oxide collapsed upon thermal treatment due to poor cross-linking of the inorganic framework and its redox properties.

The use of nanoparticles as building blocks instead of molecular precursors is an attractive route to mesoporous metal oxides with nanocrystalline walls that display improved thermal stability and show significant promise for structure-sensitive catalytic reactions. Ying et al.[133] have employed colloidal ZrO_2 nanocrystals to prepare mesoporous mixed tungsten-zirconium oxide. They proposed that this self-assembly process is driven by attractive forces between negatively charged metatungstate ions (I^-), positively charged ZrO_2 nanoparticles (C^+), and hydrogen-bonded polymer surfactants (S^0H^+). The same synthesis pathway has been used successfully to prepare mesoporous tungsten-titanium oxide. Honma et al. have reported a novel methodology to prepare ordered mesoporous nanocomposites with crystalline oxide frameworks employing functional nanocrystals as the building blocks.[134] Ordered mesoporous nanocomposites consisting of electrochemically active nanocrystals and semiconductive glass in the TiO_2-P_2O_5-M_xO_y systems (where M is a metal ion) were formed. Other mesoporous mixed-metal oxides, such as Zr-Ti and Zr-W oxides, have also been reported by Stucky et al.[59,63]

3. Ordered Macroporous Oxides

3.1. Structural Characteristics

Colloidal crystals consisting of three-dimensional ordered arrays of monodispersed spheres can be used as novel templates for the preparation of highly ordered macroporous inorganic solids that exhibit precisely controlled pore sizes and highly ordered 3D porous structures. The macroscale templating approach typically consists of three steps. First, the interstitial voids of the monodisperse sphere arrays are filled with precursors of various classes of materials, such as ceramics, semiconductors, metals, monomers,

etc. In the second step, the precursors condense and form a solid framework around the spheres. Finally, the spheres are removed by either calcination or solvent extraction.

The success of forming macroporous ordered structures is mainly determined by van der Waals interactions, wetting of the template surface, filling of the voids between the spheres, and volume shrinkage of the precursors during the solidification process. The colloidal crystal templating method may be used in combination with sol-gel, salt solution, nanocrystalline, and other precursors to produce the inorganic 3D macrostructures.[6] The colloidal-crystal templates used to prepare 3D macroporous materials include monodisperse polystyrene (PS), poly(methyl methacrylate) (PMMA), and silica spheres. A typical SEM image of a colloidal array of polystyrene spheres used as a template in the synthesis of macroporous inorganic materials is shown in Figure 10. Prior to precursor infiltration, these monodisperse spheres are ordered into close-packed arrays by sedimentation, centrifugation, vertical deposition, or electrophoresis.[135] The final inorganic macroporous structure after the removal of spheres contains the ordered interconnected pore structure shown in Figure 11.

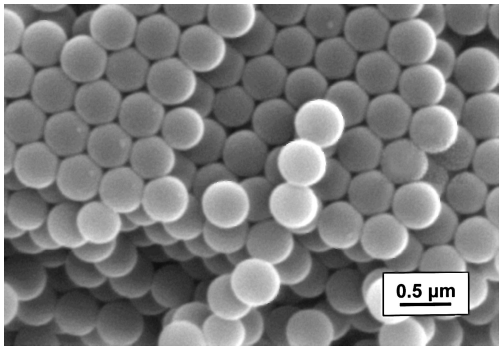

Figure 10. SEM image of an ordered array of ~400 nm polystyrene spheres.[173]

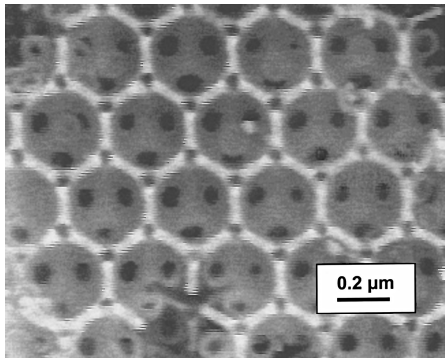

Figure 11. SEM image of a macroporous inorganic material. The walls consist of ~20 nm $(VO)_2P_2O_7$ crystals (modified from ref.[173]).

3.2. Macroporous Binary and Mixed-Metal Oxides

Several synthesis methods have been used in the past to prepare 3D macroporous inorganic materials. These include sol-gel, salt precipitation, nanocrystal infiltration, and polymerization. All these synthesis methods rely on the use of a polymeric or inorganic template, usually in a form of spheres packed in a periodic fashion. Bulk ordered transition metal macroporous oxides prepared by the sol-gel[136–145] and other methods[146–158] are summarized in Table 5 and Table 6, respectively. The most representative methods to prepare inorganic macrostructures are briefly discussed below.

Macroporous inorganic frameworks have been successfully prepared using the sol-gel method, in which metal alkoxides dissolved in alcohol are impregnated into the voids of the colloidal (polymer) sphere arrays. Hydrolysis and condensation take place at the sphere surface to form the inorganic framework. Subsequent heat treatment to remove the polymer spheres results in an ordered macroporous metal oxide. The final macropore dimensions are about 15–30 % smaller than those of the original spheres due to the shrinkage of the inorganic framework. This is caused by a large volume loss during the sol-gel process as the alcohol is evaporated. Significant shrinkage of the inorganic framework during template removal by heat treatment results in severe cracking and loss of long-range order. Therefore the sol-gel method, in combination with heat treatment to remove polymer spheres, has not resulted to date in highly ordered macroporous materials for photonic bandgap applications, for which long-range order is required. Several single, binary, and tertiary oxides have been prepared using sol-gel chemistry: SiO_2;[136] TiO_2, ZrO_2, SiO_2;[137] TiO_2, ZrO_2, Al_2O_3;[138] SiO_2, TiO_2, ZrO_2, Al_2O_3, Fe_2O_3, Sb_4O_6,

Table 5. Macroporous transition-metal oxides prepared using colloidal sphere templates by a sol-gel method.

Colloidal template	Macroporous framework	Pore structure	Ref.
ca. 0.35 µm oil microemulsion droplets	TiO_2, ZrO_2	> 50 nm hcp	Imhof and Pine 1997[137]
ca. 0.47 µm ps	TiO_2, ZrO_2	320–360 nm hcp	Holland et al. 1998[138]
0.4–0.7 µm ps	TiO_2, ZrO_2, Fe_2O_3, Sb_4O_6, WO_3, $YZrO_2$	250–500 nm ffc/hcp	Holland et al. 1999[139]
ca. 0.4 µm ps	vanadium phosphorus oxides	300–400 nm hcp	Carreon and Guliants 2001[141] 2002[142]
ca. 1 µm ps	TiO_2, ZrO_2, $PbTiO_3$, $Pb(ZrTi)O_3$	disordered hcp 800–1000 nm	Gundiah and Rao 2000[143]
0.64 µm ps	TiO_2, ZrO_2	disordered hcp ~400 nm	Wang et al. 2001[145]

Table 6. Macroporous transition metal oxides prepared using colloidal sphere templates by other synthesis methods.

Colloidal template	Macroporous framework	Pore structure	Synthesis method	Ref.
0.36–2.92 μm ps	TiO_2	240–2000 nm hcp	liquid phase chemical reaction	Wijnhoven and Vos 1998[146]
ca. 0.4–0.7 μm ps	NiO	250–500 nm hcp	salt precipitation and chemical conversion	Yan et al. 1999[147]
0.6–0.8 μm ps	MgO, NiO, Cr_2O_3, Mn_2O_3, Fe_2O_3, Co_3O_4,	380–550 nm hcp	salt precipitation and chemical conversion	Yan et al. 2000[148]
0.56 μm ps	TiO_2	320–525 nm fcc	nanocrystal incorporation	Subramanian et al. 1999[149]
0.33 μm ps/0.336 μm silica spheres 0.33 μm pmma/0.336 μm silica spheres	TiO_2, ZrO_2	ca. 270–330 nm hcp	inverse opal templating	Colvin et al. 2001[158]

WO_3, $YZrO_2$;[139] SiO_2;[140] V-P-O;[141,142] SiO_2, TiO_2, ZrO_2, $PbTiO_3$, $Pb(ZrTi)O_3$;[143] Eu_2O_3, Nd_2O_3, Sm_2O_3;[144] TiO_2, TiO_2/SiO_2;[145] TiO_2.[146]

Precipitation of metal salts, such as acetates and oxalates, and oxides within the colloidal polymer-sphere arrays, and subsequent chemical conversion of the inorganic precursors, is an alternative method to prepare ordered macroporous structures. This procedure is less sensitive to atmospheric humidity and allows the formation of ordered 3D macroporous structures for compositions difficult to prepare by sol-gel techniques. Yan et al.[147] have reported the synthesis of macroporous NiO with 250–500 nm voids by templated precipitation and subsequent chemical conversion of the inorganic precursors. The metal salt solution (acetates or nitrates) penetrates the void spaces between the spheres, and subsequent calcination of the macrocomposite removes the spheres and produces the desired metal oxide. A number of ordered macroporous inorganic oxides have been prepared by the salt precipitation method: MgO, Cr_2O_3, Mn_2O_3, Fe_2O_3, Co_3O_4.[148]

Ordered macroporous materials may be prepared by filling the void spaces of colloidal sphere arrays with nanoparticles. This method offers the great advantage of incorporating specific nanoparticles of desirable crystalline phases into the wall structure of the macroporous framework. Another major advantage of this method is that it results in very little shrinking and cracking of the 3D framework during template removal. Typically, the pore shrinkage is limited to 5–10 %. Subramania et al.[149] have used monodisperse PS spheres to template colloidal dispersions of silica and titania and form 3D structures with 320–525 nm macropores. Vlasov et al.[150] have used CdSe nanocrystals templated against monodisperse silica spheres to synthesize macroporous CdSe semiconductors.

Polymerization of organic precursors around colloidal silica-sphere arrays is a common method to produce ordered macroporous polymeric materials. The colloidal arrays of spheres are filled with a liquid monomer, which is subsequently polymerized by heat treatment or UV irradiation. Macroporous polyurethane, poly(acrylate/methacrylate), PMMA, polystyrene, epoxy, and poly(methyl acrylate) have been prepared using this methodology.[151–153]

Other miscellaneous techniques for the preparation of inorganic macrostructures include spraying techniques,[154,159] electrodeposition,[155–157,160] and inverse opal templating.[152,158] Spraying techniques have been used mainly in the preparation of macroporous films. Macroporous TiO_2, for example, has been prepared by spray pyrolysis by depositing titanyl acetylacetonate onto silica spheres,[154] and macroporous Au has been synthesized by ion spraying.[159] Electrodeposition techniques offer excellent control over the degree of filling and wall thickness. Growth of the desirable macrostructure occurs galvanostatically or potentiostatically. Macrostructures of CdS, CdSe,[155,156] ZnO,[160] polypyrrole, polyaniline, and poly(bithiophene)[157] have been successfully prepared by electrodeposition. In the inverse opal templating method, 3D macroporous structures prepared by templating with opal structures can be subsequently used to form another opal replica. A wide range of compositions, (TiO_2, ZrO_2, Al_2O_3, polypyrrole, PPV (polyphenylene-vinylene), CdS, AgCl, Au, Ni) [158] have been prepared by this method.

Macroporous vanadium-phosphorus-oxide (VPO) phases with remarkable compositional, structural, and morphological properties have been synthesized by employing monodisperse polystyrene sphere arrays as a template.[141,142] Colloidal polystyrene spheres were ordered into closed-packed arrays by sedimentation or centrifugation. Depending on the choice of VPO source and template-removal method, various crystalline VPO phases were obtained. The macroscale-templated synthesis produced VPO phases with unprecedentedly high surface areas (75 m^2/g), desirable macroporous architectures, optimal bulk compositions (P/V ≈ 1.1), desirable vanadium oxidation states (+4.1 to +4.4), and preferential exposure of the surface (100) planes of vanadyl(IV) pyrophosphate, $VO_2P_2O_7$, which is the proposed active and selective phase for *n*-butane oxidation to maleic anhydride.

The ability to control wall thickness, pore size, and elemental and phase compositions makes colloidal sphere array templating a versatile, attractive, and flexible route for the synthesis of highly ordered macroporous materials with fine-tuned pore and framework architectures. The wall thickness of macroporous structures can be controlled by the hydrolysis/condensation rates of the inorganic precursors,[139] the packing of the PS spheres,[142] and by forming core-shell structures at the sphere surface (i.e. deposition of polyelectrolyte multilayers at the sphere surface).[145] The pore size can be easily manipulated in the range of the sphere sizes, which are typically between 100 nm and 50 μm

in diameter. Even smaller spheres (20 nm) can be prepared and used to template small-pore materials.[6] Furthermore, it is possible to build macroporous structures containing a specific crystalline phase by incorporating nanoparticles of desired phases in the voids of sphere arrays.[149,150] Depending on the choice of the inorganic sources and template-removal method, various crystalline phases can be obtained.[142] This suggests that the most critical aspects in the preparation of these macroporous structures are the ability of the precursors to infiltrate and condense between the spaces of the colloidal spheres without swelling or destroying the template, as well as the ability to avoid excessive grain growth, as this leads to a decrease in macroporosity and structural order.

4. Emerging Catalytic Applications

4.1. Mesoporous Metal Oxides

Finely tuned pore sizes, metal oxide wall structures and compositions, high surface areas, and enhanced accessibility of the active surface sites in ordered mesoporous metal oxides are highly attractive for diverse catalytic applications. A thorough review of emerging applications of mesoporous transition metal oxides in catalysis is given here. Reported examples of catalytic mesoporous metal oxides are summarized in Table 7.

Some early examples of catalytic mesoporous silicates have been reviewed by Sayari.[159] More recently, Ogawa et al.[160] have reported the use of Al-containing mesoporous silica films as nanoreactors for organic photochemical reactions. An adsorbed azobenzene derivative incorporated in the film exhibited photochemical isomerization upon UV/Vis irradiation at temperatures as low as 80–300 K. However, no comparison with conventional nonmesoporous systems was conducted. Ikeue et al.[161] have reported Ti-containing porous silica films that exhibit high photocatalytic activity in the reaction of CO_2 with H_2O to produce CH_4 and CH_3OH as the main products. The quantum yield of these mesoporous Ti-silica films was 0.28 %, which is significantly higher than the value of 0.02 % obtained with titanium oxides anchored on a transparent porous silica glass (PVG). Such improvement in the reactivity may be attributed to the higher surface area and ordered pore structure of the mesoporous Ti-silica films. Soga et al.[162] have prepared aluminoxanes adsorbed on mesoporous silica that display ethylene polymerization activity in a catalytic system containing bis(cyclopentadienyl)zirconium dichloride. Furuya et al.[163] have used Ti-mesoporous silica to oxidize cyclohexene to cyclohexene oxide with *t*BuOOH in the presence of benzene and cyclohexane with 99 % selectivity at 98 % conversion. Methanol oxidation over Nb_2O_5/SiO_2 and Nb/MCM-41 has been studied by Wachs et al.[164] Although their results showed that the dispersed Nb species in both catalysts were the active and selective sites for methanol oxidation, Nb/MCM-41 displayed higher overall activity due to a better dispersion of isolated NbO_4 species per unit mass of this catalyst.

Only a few reports exist on catalytic applications of mesoporous transition metal oxides. Yussuf et al.[165] have reported the photocatalytic behavior of mesoporous titania films. They found that the photocatalytic activity of the films for the oxidation of NO_x was higher for the mesoporous films than for conventional gel films, probably due to

Table 7. Emerging catalytic applications of mesoporous metal oxides.

Oxide system[a]	Reaction	Product	Reaction conditions	Activity/ selectivity	Ref.
TiO_2	NO photooxidation	NO_2	black light intensity 10 mW/m^2 (λ = 365 nm), 1 ppm NO in 50 % rel. humidity air at 3.0 L/min	15 % NO removal, 10 % NO_2 generation	[165]
NiO-Ta_2O_5	photocatalytic water decomposition	$H_2 + O_2$	0.5 g 4 wt.-% NiO/Ta_2O_5 in 400 mL H_2O, irradiated by high pressure Hg lamp (450 W)	515 μmol/h H_2, 272 μmol/h O_2	[166]
PO_3-TiO_2-Nb_2O_5	2-propanol dehydrogenation	acetone	0.4 g catalyst in 50 mL 1:1 2-propanol/H_2O mixture sparged by 2 mL/min O_2 and irradiated by 150 W Xe lamp	quantum yields[b]: 0.0089 (**TiO_2**) 0.45 (Degussa P25) 0.0041 (**Nb_2O_5**) 0.217 (Nb_2O_5)	[167]
Fe_2O_3-TiO_2	cyclohexane oxidation	cyclohexanol, cyclohexanone, isobutyraldehyde, acetic acid	T = 343 K p = 1 atm time = 15–17 h	conversion = 25.8 % selectivity to cyclohexanol and cyclohexanone = 90 %	[168]
VO_x -TiO_2	propene oxidation	CO + CO_2	T = 500 K p_{O_2} = 6.6 kPa $p_{C_3H_6}$ = 2.4 kPa	activity (min^{-1}) CO = 0.091 CO_2 = 0.279 select. to CO_2 = 75 %	[169]
VPO	*n*-butane oxidation	maleic anhydride	T = 673 K 1.7 % *n*-butane in air space velocity F/V = 55 min^{-1}	*n*-butane conversion = 10 % selectivity to maleic anhydride = 40 %	[121]

[a] Letters in bold refer to the mesoporous oxides. [b] Quantum yield is defined as the molecules of acetone formed per incident photon.

the higher surface areas of the mesoporous films. In a different study,[166] mesoporous Ta_2O_5 doped with NiO was found to display higher photocatalytic activity than nonporous amorphous and crystalline NiO-Ta_2O_5. It was claimed that the higher surface areas and better NiO dispersion over the mesoporous Ta_2O_5 host were responsible for the superior catalytic performance of these materials. The photocatalytic activity of mesoporous phosphated titanium and niobium oxide catalysts has been studied in the dehydrogenation of 2-propanol to acetone.[167] Surprisingly, a lower activity of the mesoporous Ti and Nb oxides was observed than for the bulk anatase phase. The amorphous nature of the mesoporous walls and the surface defects in these mesoporous oxides are probably responsible for the recombination of photogenerated electron-hole pairs and the poor catalytic performance.

Gedanken et al.[168] have studied the oxidation of cyclohexane to cyclohexanol and cyclohexanone over a mesoporous Fe_2O_3-TiO_2 catalyst. The mesoporous catalysts displayed about a 5 % higher cyclohexane conversion under the same conditions as compared to catalysts in which Fe_2O_3 was incorporated into nonporous TiO_2. Yoshitake and Tatsumi[169] have incorporated vanadium oxide into mesoporous TiO_2 and studied these novel catalysts in propene oxidation reaction. They found that the rate of propane oxidation to CO and CO_2 was about 18 times higher with mesoporous VO_x-TiO_2 catalysts than with conventional VO_x-TiO_2 (i.e. a nonporous TiO_2 matrix). The high surface areas displayed by these mesoporous catalysts and improved dispersion of active surface sites in the mesoporous hosts are responsible for their enhanced catalytic performance.

The catalytic performance of ordered mesostructured vanadium-phosphorus-oxides in selective *n*-butane oxidation has been studied by Carreon and Guliants.[121] Mesostructured VPO was evaluated in the oxidation of *n*-butane to maleic anhydride. Selectivities to maleic anhydride of up to 40 mol-% were observed at 673 K at about 10 % *n*-butane conversion. A conventional organic VPO catalyst containing well-crystallized vanadyl(IV) pyrophosphate, the proposed active and selective phase for *n*-butane oxidation to maleic anhydride, displayed selectivities to maleic anhydride of 50 mol-% under the same reaction conditions. The limited thermal stability of mesostructured VPO during *n*-butane oxidation led to the gradual loss of the structural order and poor catalytic performance. These results further suggested that crystalline vanadyl(IV) pyrophosphate is required for this alkane oxidation reaction.

Other potential applications of mesoporous metal oxides, such as in fuel cells, as semiconductors, cathode materials, superparamagnets, etc., have been discussed recently by He and Antonelli[170] and are outside the scope of this review.

4.2. Macroporous Metal Oxides

Ordered macroporous films and membranes are novel monolithic materials with potential applications in heterogeneous catalysis, bioseparations, as well as membrane supports for the separation of small molecules. Due to their high surface area (up to 230 m^2/g) and unimodal large pores, these macroporous structures are highly attractive for a variety of separation and catalytic applications involving large molecules.

Only a few examples of catalytic applications have been reported for bulk macroporous solids. Stein et al.[171,172] have used ordered macroporous silica as a support for catalytically active species. For instance, they found that γ-$SiW_{10}O_{36}$ polyoxometalate clusters incorporated into the walls of macroporous silica exhibit catalytic activity for the epoxidation of cyclooctene.[171] In another study, they[172] compared different pore structures (macro, meso and nonporous silica surfaces) with the activity of silica samples doped with transition-metal-substituted polyoxometalates (TMSPs). Although the three types of catalysts showed comparable conversions in the epoxidation of cyclohexene to cyclohexene oxide, the open macroporous structure supported a greater number of TMSP clusters at its surface, thus leading to improved cluster retention during the catalytic reaction. The recently reported macroporous VPO represents the first example of a macroporous transition mixed-metal oxide employed in the selective oxidation of lower alkanes.[173] The catalytic performance of this VPO phase was evaluated in the partial oxidation of *n*-butane to maleic anhydride. The observed yield of maleic anhydride was greater than 50 % for macroporous VPO.[173] Under similar reaction conditions, the yield of maleic anhydride was about 40 % for the conventional organic VPO catalyst. The ordered open-pore structures, the high surface areas (>40 m^2/g), and the presence of nanocrystalline $(VO)_2P_2O_7$ in macroporous VPO resulted in improved catalytic performance. The successful preparation of these catalytically active bulk phases ushers in new and exciting opportunities for the design of macroporous films and membranes for various applications in biocatalysis and bioseparations. Other nanotechnological applications of these novel meso- and macroporous metal-oxide phases have been recently reviewed.[18]

5. Concluding Remarks

The present review of mesostructured binary and mixed-metal oxides demonstrates that complete surfactant removal and the attainment of high thermal stability are some of the critical challenges in the synthesis of mesoporous metal oxides. Incomplete cross-linking of the inorganic frameworks, strong covalent bonds between the inorganic species and surfactant molecules, the rigidity of the M–O–M bond angles, the low Tammann temperature of the constituent metal oxides, and bulk redox reactions are among the most notable causes of the limited thermal stability of mesoporous binary and mixed-metal oxides.

Several synthetic strategies are promising to overcome the limited thermal stability of mesostructured transition metal oxides. One proposed strategy is to strengthen the

inorganic framework by increasing cross-linking with silicate[89] and phosphate[174] species prior to surfactant removal. Another strategy consists in avoiding strong electrostatic interactions at the organic–inorganic interface, instead directing the synthesis through weak hydrogen-bonding interactions, and consequently improving the thermal stability of the final mesostructure.[59,63]

Furthermore, the lattice oxygen mobility during surfactant combustion may be lowered and, as a result, the thermal stability of the mesostructure improved by employing oxides with high Tammann temperatures (Table 1). For example, Nb_2O_5 [61,62] and ZrO_2 [80] mesostructures with relatively high Tammann temperatures (Table 1) display good thermal stability. Similarly, thermally stable mesoporous mixed-metal oxides may be obtained by employing oxides with a high Tammann temperature as the major structural component. For instance, thermally stable mesoporous V-Mg oxide,[112,113] V-Nb oxide,[123] and Y_2O_3-ZrO_2 [138] have been successfully prepared. In all these cases oxides with high Tammann temperature (i.e. Mg, Nb, and Zr oxides) were used as the major component in the mixed-metal oxide system.

The use of a liquid crystalline L_3 phase represents another attractive alternative for the preparation of mesoscopic mixed-metal oxides with open-pore structures without the need for surfactant removal. The L_3 phase consists of a surfactant bilayer forming a sponge-like structure with randomly distributed mesopores interconnected in all three dimensions.[175,176] The pore diameter in the L_3 phase increases with increasing solvent content, thus providing a procedure by which the pore diameter can be tuned to a specific size. Only the solvent, rather than the surfactant molecules, occupies the primary pore volume. Therefore, the void space is immediately available for the condensation of an inorganic framework without the need to remove the surfactant. The only limitation of this approach is that the resultant mesostructures must be used at temperatures below the surfactant decomposition temperature (i.e. about 600 K) to avoid the collapse of the mesostructure.

For many structure-sensitive catalytic applications, such as the selective oxidation of lower alkanes over bulk mixed-metal oxides, it is highly desirable to have a well-defined crystalline catalytic phase. Therefore, the self-assembly of nanocrystalline building blocks into mesostructured metal-oxide phases represents a highly promising method to prepare mesoporous metal oxides with nanocrystalline walls.[140] In this respect, the macroscale-templated synthesis of nanocrystalline mixed-metal oxides is an attractive approach for the design of catalytic phases that possess remarkable ordering on the macroscale (>50 nm for pore architectures) displaying nanocrystalline walls.

Meso- and macroscale self-assembly approaches are particularly attractive for the design of novel catalytic phases on multiple length-scales that possess unique pore structures, flexible compositions, and tunable surface active sites. These unique porous structures with finely tuned surface active sites are highly promising as improved catalysts for a variety of selective alkane oxidation reactions. Moreover, it is expected that these novel model catalytic systems would lead to an improved fundamental understanding of the relationships between the molecular structure and catalytic properties of a broad range of industrially relevant catalytic systems.

[1] C. T. Kresge, M. E. Leonowicz, W. J. Roth, J. C. Vartuli, J. S. Beck, *Natur e* **1992**, *359*, 710.
[2] J. S. Beck, J. C. Vartuli, W. J. Roth, M. E. Leonowicz, C. T. Kresge, K. D. Schmitt, C. T.-W. Chu, D. H. Olson, E. W. Sheppard, S. B. McCullen, J. B. Higgins, J. L. Schlenker, *J. Am. Chem. Soc.* **1992**, *114*, 10834.
[3] C. T. Kresge, M. E. Leonowicz, W. J. Roth, J. C. Vartulli J. C. (Mobil Oil Corp.) US Patent 5098684, **1992**.
[4] F. Schüth, *Chem. Mater.* **2001**, *13*, 3184.
[5] A. T. Bell, *Science* **2003**, *299*,1688.
[6] A. Stein, R. C. Schroden, *Curr. Opin. Solid State Mater. Sci.* **2001**, *65*, 553.
[7] S. Inagaki, Y. Fukushima, K. Kuroda, *J. Chem. Soc. Chem. Commun.* **1993**, 680.
[8] Q. Huo, D. I. Margolese, G. D. Stucky, *Chem. Mater.* **1996**, *8*, 1147.
[9] R. Ryoo, J. M. Kim, C. H. Ko, C. H. Shin, *J. Phys. Chem.* **1996**, *100*, 17718.
[10] S. A. Bagshaw, E. Prouzet, T. J. Pinnavaia, *Scienc e* **1995**, *269*, 1242.
[11] W. Zhou, J. Klinowski, *Chem. Phys. Lett.* **1998**, *292*, 207.
[12] D. Zhao, Q. Huo, J. Feng, B. F. Chmelka, G. D. Stucky, *J. Am. Chem. Soc.* **1998**, *120*, 6024.
[13] D. Zhao, J. Feng, Q. Huo, N. Melosh, G. H. Fredickson, B. F. Chmelka, G. D. Stucky, *Scienc e* **1998**, *279*, 548.
[14] C. J. Brinker, *Curr. Opin. Solid State. Mater. Sci* . **1996**, *1*, 798.
[15] J. C. Vartuli, C. T. Kresge, W. J. Roth, S. B. McCullen, J. S. Beck, K. D. Schmitt, M. E. Leonowicz, J. D. Lutner, E. W. Sheppard, in Advanced Catalysts and Nanostructured Materials: Modern Synthesis Methods (Ed.: W. R. Moser), Academic Press, New York, **1996**.
[16] G. D. Stucky, Q. Huo, A. Firouzi, B. F. Chmelka, S. Schacht, I. G. Voigt-Martin, F. Schüth, *Studies in Surface Science and Catalysis* **1997**, *105*, 3.
[17] N. K. Raman, M. T. Anderson, C. J. Brinker, *Chem. Mater.* **1996**, *8*, 1682.
[18] V. V. Guliants, M. A. Carreon, Y. S. Lin, *J. Membr. Sci.* **2004**, *235*, 53.
[19] G. J. de A. A. Soler-Illia, C. Sanchez, B. Lebeau, J. Patarin, *Chem. Rev.* **2002**, *102*, 4093.
[20] C. Y. Chen, S. L. Burkett, H. X. Li, M. E. Davis, *Microlithogr. World Micropor. Mater.* **1993**, *2*, 27.
[21] A. Steel, S. W. Carr, M. W. Anderson, *J. Chem. Soc. Chem. Commun.* **1994**, 1571.
[22] A. Monnier, F. Schüth, Q. Huo, D. Kumar, D. Margolese, R. S. Maxwell, G. D. Stucky, M. Krishnamurty, P. Petroff, A. Firouzi, M. Janicke, B. F. Chmelka, *Scienc e* **1993**, *261*, 1299.
[23] G. D. Stucky, A. Monnier, F. Schüth, Q. Huo, D. Margolese, D. Kumar, M. Krishnamurty, P. Petroff, A. Firouzi, M. Janicke, B. F. Chmelka, *Mol. Cryst. Liq. Cryst.* **1994**, *240*, 187**.**
[24] A. Firouzi, D. Kumar, L. M. Bull, T. Besier, R. Sieger, Q. Huo, S. A. Walker, J. A. Zasadzinski, C. Glinka, J. Nicol, D. Margolese, G. D. Stucky, B. F. Chmelka, *Scienc e* **1995**, *267*, 1138.
[25] S. Ikeda, in Surfactants in Solution, vol. 2 (Eds.: K. L. Mittal, B. Lindman), Plenum, New York, **1984**, 825.
[26] A. Firouzi, F. Atef, A. G. Oertli, G. D. Stucky, B. F. Chmelka, *J. Am. Chem. Soc.* **1997**, *119*, 3596.
[27] O. Regev, *Langmui r* **1996**, *12*, 4940.
[28] J. Frasch, B. Lebeau, M. Soulard, L. Patarin, R. Zana, *Langmuir* **2000**, *16*, 9049.
[29] M. Tiemann, V. Goletto, R. Blum, F. Babonneau, H. Amenitsch, M. Linden, *Langmui r* **2002**, *18*, 1005.

[30] J. Patarin, B. Lebeau, R. Zana, *Current Opinion in Colloids & Interface Science* **2002**, *7*, 107.
[31] K. Flodstroem, C. V. Teixeira, H. Amenitsch, V. Alfredsson, M. Linden, *Langmuir* **2004**, *20*, 12, 4885.
[32] R. J. Hunter, *Zeta potential in colloid science: principles and applications*, Academic Press, London, New York, **1981**.
[33] G. A. Parks, *Chem. Rev.* **1965**, *65*, *2*, 17.
[34] T. J. Gray, D. P. Detwiler, D. E. Rase, W. G. Lawrence, R. R. West, T. J. Jennings, *The Defect Solid State*, Interscience, New York, **1957**, p. 96.
[35] *CRC Handbook of Chemistry and Physics: A Ready-Reference Book of Chemical and Physical Data* (Ed.-in-Chief: R. C. Weast; Associate Eds.: M. J. Astle, W. H. Beyer), 67th ed., CRC Press, Boca Raton, FL, **1986**.
[36] M. M. Lin, *Appl. Catal.* **2001**, *207*(1–2), 1.
[37] G. Centi, *Catal. Today* **1993**, *16–18*, 16.
[38] M. Hatano, A. Kayo, EP Patent 318,295 A1, **1988**.
[39] T. Ushikubo, K. Oshima, T. Umezawa, K. Kiyono, EP Patent 512,846 A1, **1992**.
[40] K. Oshima, A. Kayo, T. Umezawa, K. Kiyono, I. Sawaki, EP Patent 529, 853 A2, **1992**.
[41] G. Centi, F. Trifiro, *Catal. Rev. Sci. Eng.* **1986**, *28*, 165.
[42] R. K. Grasselli, *Catal. Today* **1999**, *49*, 141.
[43] P. Concepcion, J. M. Lopez Nieto, J. Perez-Pariente, *J. Mol. Catal. A: Chem.* **1995**, *99*, 173.
[44] E. A. Mamedov, V. C. Corberan, *Appl. Catal. A* **1995**, *127*, 1.
[45] R. Catani, G. Centi, F. Trifiro, R. K. Grasselli, *Ind. Eng. Chem. Res.* **1992**, *31*, 107.
[46] M. Bettahar, G. Costentin, L. Savary, J. Lavalley, *Appl. Catal. A* **1996**, *145*, 1.
[47] D. J. Hucknall, Selective Oxidation of Hydrocarbons, Academic Press, London **1974**.
[48] S. T. Oyama, A. N. Desikan, J. W. Hightower, Catalytic Selective Oxidation, ACS Symposium Series 523, American Chemical Society: Washington DC **1993**.
[49] J. Haber, *Stud. Surf. Science Catal*. **1997**, *110*, 1; (3rd World Congress on Oxidation Catalysis).
[50] G. Centi, F. Cavani, F. Trifiro, Selective Oxidation by Heterogeneous Catalysis. Fundamental and Applied Catalysis, Kluwer Academic/Plenum Publishers, New York, **2001**.
[51] J. L. G. Fierro, L. A. Arrua, J. M. Lopez Nieto, G. Kremenic, *Appl. Catal.* **1988**, *37*, 323.
[52] D. A. Bulushev, L. Kiwi-Minsker, V. I. Zaikovskii, A. Renken, *J. Catal.* **2000**, *193*,145.
[53] G. S. Wong, D. D. Kragten, J. M. Vohs, *J. Phys. Chem. B* **2001**, *105*, 1366.
[54] N.-Y. Topsoe, H. Topsoe, J. A. Dumesic, *J. Catal.* **1995**, *151*, 226.
[55] H. Roussel, B. Mehlomakulu, F. Belhadj, E. Van Steen, J. M. Millet, *J. Catal.* **2002**, *205*, 97.
[56] V. Luca, D. J. MacLachlan, J. M. Hook, R. Withers, *Chem. Mater.* **1995**, *7*, 2220.
[57] G. G. Janauer, A. Dobley, J. Guo, P. Zavalij, M. S. Whittingham, *Chem. Mater.* **1996**, *8*, 2096.
[58] P. Liu, I. L. Moudrakouski, J. Liu, A. Sayari, *Chem. Mater.* **1997**, *9*, 2513.
[59] P. Yang, D. Zhao, D. I. Margolese, B. F. Chmelka, G. D. Stucky, *Chem. Mater.* **1999**, *11*, 2813.
[60] P. Liu, S.-H. Lee, C. E. Tracy, Y. Yan, J. A. Turner, *Adv. Mater.* **2002**, *14*, *1*, 27.
[61] D. M. Antonelli, A. Nakahira, J. Y. Ying, *Inorg. Chem.* **1996**, *35*, 3126.
[62] D. M. Antonelli, J. Y. Ying, *Angew. Chem. Int. Ed. Engl.* **1996**, *35*, *4*, 426.
[63] P. Yang, D. Zhao, D. I. Margolese, B. F. Chmelka, G. D. Stucky, *Natur e* **1998**, *396*, 152.
[64] A. Fujishima, K. Hinda, *Natur e* **1972**, *238*, 37.
[65] Z. B. Zhang, C. C. Wang, R. Zakaria, J. Y. Ying, *J. Phys. Chem. B* **1998**, *102*, 10871.
[66] F. Lonyi, J. Valyon, J. Engelhardt, F. Mizukami, *J. Catal.* **1996**, *160*, 279.
[67] T. Yamaguchi, *Appl. Catal.* **1990**, *61*, 1.
[68] X. Bokhimi, A. Morales, O. Novaro, T. Lopez, E. Sanchez, R. Gomez, *J. Mater. Res.* **1995**, *10*,*11*, 2788.
[69] D. T. On, *Langmui r* **1999**, *15*, 8561.
[70] D. Khushalani, G. A. Ozin, A. Kuperman, *J. Mater. Chem.* **1999**, *9*, 1491.
[71] W. S. Postula, Z. Feng, C. V. Philip, A. Akgerman, R. G. Anthony, *J. Catal.* **1994**, *145*, 126.
[72] Z. Feng, W. S. Postula, C. V. Philip, R. G. Anthony, *J. Catal.* **1994**, *148*, 84.
[73] A. F. Bedilo, K. J. Klabunde, *J. Catal.* **1998**, *176*, 448.
[74] C. Morterra, G. Cerrato, F. Pinna, M. Signoretto, G. Strukul, *J. Catal.* **1994**, *149*,181.
[75] F. R. Chen, G. Coudurier, J. F. Joly, J. C. Vedrine, *J. Catal.* **1993**, *143*, 616.
[76] M. A. Risch, E. E. Wolf, *Appl. Catal. A* **1998**, *172*, L1.
[77] C. Morterra, G. Cerrato, F. Pinna, M. Signoretto, *J. Catal.* **1995**, *157*, 109.
[78] K. Arata, *Adv. Catal.* **1990**, *37*, 165.
[79] C. Morterra, G. Cerrato, C. Emanuel, V. Bolis, *J. Catal.* **1993**, *142*, 349.
[80] M. S. Wong, J. Y. Ying, *Chem. Mater.* **1998**, *10*, 2067.
[81] X. Song, A. Sayari, *Catal. Rev. Sci. Eng.* **1996**, *38*, 329.
[82] P. Liu, J. Liu, A. Sayari, *Chem. Commun.* **1997**, 577.
[83] I. E. Wachs, Y. Chen, J.-M. Jehng, L. E. Briand, T. Tanaka, *Catal. Today* **2003**, *78*, 13.
[84] M. Hara, G. Hitoki, T. Takata, J. N. Kondo, H. Kobayashi, K. Domen, *Catal. Today* **2003**, *78*, 555.
[85] H. Kato, A. Kudo, *Catal. Today* **2003**, *78*, 561.
[86] D. M. Antonelli, J. Y. Ying, *Chem. Mater.* **1996**, *8*, 874.
[87] G. M. Panjok, *Appl. Catal.* **1991**, *72*, 217.
[88] Z. R. Tian, W. Tong, J. Y. Wang, N. G. Duan, V. V. Krishnan, S. L. Suib, *Scienc e* **1997**, *276*, 926.
[89] X. Liu, C.-M. Chun, I. A. Aksay, W.-H. Shih, *Ind. Eng. Chem. Res.* **2000**, *39*, 684.
[90] J. Luo, S. L. Siub, *Chem. Commun.* **1997**, 1031.
[91] M. Yada, H. Kitamura, M. Machida, T. Kijima, *Inorg. Chem.* **1998**, *37*, 6470.
[92] M. Froba, O. Muth, *Adv. Mater.* **1999**, *11*, *7*, 564.
[93] B. J. Liaw, D. S. Cheng, B. L. Yang, *J. Catal.* **1989**, *118*, 312.
[94] B. L. Yang, M. C. Kung, H. H. Kung, *J. Catal.* **1984**, *89*, 172.
[95] F. Hong, B. L. Yang, L. H. Schwartz, H. H. Kung, *J. Phys. Chem.* **1984**, *88*, 2525.
[96] D. N. Srivastava, N. Perkas, A. Gedanken, I. Felner, *J. Phys. Chem. B* **2002**, *106*, *8*, 1878.
[97] Y. Wang, L. Yin, A. Gedanken, *Ultrason. Sonochem.* **2002**, *9*,*6*, 285.
[98] P. Yang, *J. Chromatogr. Libr. Monolith. Mater.* **2003**, *67*, 301.
[99] S. Polarz, B. Smarsly, *J. Nanosci. Nanotech.* **2002**, *2*,*6*, 581.
[100] K. Moller, T. Bein, *Chem. Mater.* **1998**, *10*, 2950.
[101] V. V. Guliants, J. B. Benziger, S. Sundaresan, I. E. Wachs, J. M. Jehng, J. E. Roberts, *Catal. Today* **1996**, *28*, 275.
[102] R. M. Contractor, US Patent 4 668 802 to E. I. DuPont de Nemours and Company **1987**.
[103] R. M. Contractor, H. S. Horowitz, G. S. Patience, J. D. Sullivan, US Patent 5 895 821 to E. I. DuPont de Nemours and Company **1999**.
[104] U. Rodemerck, B. Kubias, H. W. Zanthoff, G. U. Wolf, M. Baerns, *Appl. Catal. A* **1997**, *153*, 217.
[105] G. Centi, F. Trifirò, J. R. Ebner, V. M. Franchetti, *Chem. Rev.* **1988**, *88*, 55.
[106] E. M. Thornsteinson, T. P. Wilson, F. G. Young, P. H. Kasai, *J. Catal.* **1978**, *52*, 116.
[107] K. Ruth, R. Burch, R. Kieffer, *J. Catal.* **1998**, *175*, 27.
[108] M. Takahashi, X. Tu, T. Hirose, M. Ishii, M. US Patent 5994580, assigned to Toagosei Co. Ltd., Japan **1999**.
[109] J. N. Al-Saeedi, V. V. Guliants, *Appl. Catal. A* **2002**, *237*, *1–2*, 111.

[110] M. O. Guerrero-Perez, J. L. G. Fierro, M. A. Vicente, M. A. Bañares, *J. Catal.* **2002**, *206*, 339.
[111] M. O. Guerrero-Perez, J. L. G. Fierro, M. A. Bañares, *Catal. Today* **2003**, *78*, *1–4*, 387.
[112] Z-S.Chao, E. Ruckenstein, *Langmui r* **2002**, *18*, 734.
[113] Z-S. Chao, E. Ruckenstein, *Langmui r* **2002**, *18*, 8535.
[114] T. Abe, A. Taguchi, M. Iwamoto, *Chem. Mater.* **1995**, *7*, 1429.
[115] T. Doi, T. Miyake, *Chem. Commun.* **1996**, 1635.
[116] J. E. Haskouri, M. Roca, S. Cabrera, J. Alamo, A. Beltran-Porter, D. Beltran-Porter, M. D. Marco, P. Amoros, *Chem. Mater.* **1999**, *11*, 1446.
[117] N. Mizuno, H. Hatayama, S. Uchida, A. Taguchi, *Chem. Mater.* **2001**, *13*, 179.
[118] M. A. Carreon, V. V. Guliants, *Microporous Mesoporous Mater.* **2002**, *55*, *3*, 297.
[119] M. A. Carreon, V. V. Guliants, *Stud. Surf. Sci. Catal.* **2002**, *141*, 301.
[120] M. A. Carreon, V. V. Guliants, *Catal. Today* **2003**, *78*, 303.
[121] M. A.Carreon, V. V. Guliants, F. Pierelli, F. Cavani, *Catal. Lett.* **2004**, *92*, *1–2*, 11.
[122] B. Lee, T. Yamashita, D. Lu, J. N. Kondo, K. Domen, *Chem. Mater.* **2002**, *14*, 867.
[123] X. He, A. Y. H. Lo, M. Trudeau, R. W. Schurko, D. Antonelli, *Inorg. Chem.* **2003**, *42*, 335.
[124] M. Thieme, F. Schüth, *Microporous Mesoporous Mater.* **1999**, *27*, 193.
[125] D. J. Jones,G. Aptel, M. Brandhorst, M. Jacquin, J. J. Jimenez, A. J. Lopez, P. M. Torres, I. Piwonski, E. R. Castellon, J. Zajac, J. Roziere, *J. Mater. Chem.* **2000**, *10*, 1957.
[126] J. Blanchard, F. Schüth, P. Thens, M. Hudson, *Microporous Mesoporous Mater.* **2000**, *39*,163.
[127] U. Ciesla, M. Froba, G. D. Stucky, F. Schuth, *Chem. Mater.* **1999**, *11*, 227.
[128] R. G. Silver, C. J. Huo, J. G. Ekerdt, *J. Catal.* **1989**, *118*, 400.
[129] C. D. Sagel-Ransijn, A. J. A. Winnubst, B. Kerkwijk, A. J. Burggraaf, H. Verweij, *J. Eur. Ceram. Soc.* **1997**, *17*, *6*, 831.
[130] P. Waldemar, *J. Eur. Ceram. Soc.* **1997**, *17*, *2–3*, 121
[131] M. Mamak, N. Coombs, G. Ozin, *J. Am. Chem. Soc.* **2000**, *122*, 8932.
[132] Y. Wang, L. Yin, O. Palchik, Y. R. Hacohen, Y. Koltypin, A. Gedanken, *Chem. Mater.* **2001**, *13*, 1248.
[133] M. S. Wong, E. S. Jeng, J. Y. Ying, *Nanoletter s* **2001**, *1*, *11*, 637.
[134] D. Li, H. Zhou, I. Honma, *Nature Mater.* **2004**, *3*,*1*, 65.
[135] Y. Xia, B. Gates, Y. Yin, Y. Lu, *Adv. Mater.* **2000**, *12*, *10*, 693
[136] a) O. D. Velev, T. A. Jede, R. F. Lobo, A. M. Lenhoff, *Natur e* **1997**, *389*, 447; b) O. D. Velev, T. A. Jede, R. F. Lobo, A. M. Lenhoff, *Chem. Mater.* **1998**, *10*, 3597.
[137] A. Imhof, D. J. Pine, *Natur e* **1997**, *389*, 948.
[138] B. T. Holland, C. F. Blanford, A. Stein, *Scienc e* **1998**, *281*, 538.
[139] B. T. Holland, C. F. Blanford, T. Do, A. Stein, *Chem. Mater.* **1999**, *11*, 795.
[140] B. T. Holland, L. Abrams, A. Stein, *J. Am. Chem. Soc.* **1999**, *121*, 4308.
[141] M. A. Carreon, V. V. Guliants, *Chem. Commun.* **2001**, 1438.
[142] M. A. Carreon, V. V. Guliants, *Chem. Mater.* **2002**, *14*, *6*, 2670.
[143] G. Gundiah, C. N. R. Rao, *Sol. State Sc.* **2000**, *2*, 877.
[144] Y. Zhang, Z. Lein, J. Li, S. Lu, *New J. Chem.* **2001**, *25*, 1118.
[145] D. Wang, R. A. Caruso, F. Caruso, *Chem. Mater.* **2001**, *13*, 364.
[146] J. E. G. Wijnhoven, W. L. Vos, *Scienc e* **1998**, *281*, 802.
[147] H. Yan, C. F. Blanford, B. T. Holland, M. Parent, W. H. Smyrl, A. Stein, *Adv. Mater.* **1999**, *11*, *12*, 1003.
[148] H. Yan, C. F. Blanford, B. T. Holland, W. H. Smyrl, A. Stein, *Chem. Mater.* **2000**, *12*, 1134.
[149] G. Subramanian, V. N. Manoharan, J. D. Thorne, D. J. Pine, *Adv. Mater.* **1999**, *11*, *15*, 1261.
[150] Y. A. Vlasov, N. Yao, D. J. Norris, *Adv. Mater.* **1999**, *11*, *2*, 165.
[151] S. H. Park, Y. Xia, *Adv. Mater.* **1998**, *10*, 1045.
[152] B. Gates, Y. Yin, Y. Xia, *Chem. Mater.* **1999**, *11*, 2827.
[153] P. Jiang, K. S. Hwang, D. M. Mittleman, J. F. Bertone, V. L. Colvin, *J. Am. Chem. Soc.* **1999**, *121*, 11630.
[154] Q. Luo, Z. Liu, L.Li, S. Xie, J. Kong, D. Zhao, *Adv. Mater.* **2001**, *13*, 286.
[155] P. V. Braun, P. Wiltzius, *Natur e* **1999**, *402*, 603.
[156] P. V. Braun, P. Wiltzius, *Adv. Mater.* **2001**, *13*, 482.
[157] P. N. Bartlett, P. R. Birkin, M. A. Ghanem, C. S. Toh, *J. Mater. Chem.* **2001**, *11*, 849.
[158] P. Jian, J. F. Bertone, V. L. Colvin, *Scienc e* **2001**, *291*, 453.
[159] A. Sayari, *Chem. Mater.* **1996**, *8*, 1840.
[160] M. Ogawa, K. Kuroda, J. Mori, *Chem. Commun.* **2000**, 241.
[161] K. Ikeue, S. Nozaki, M. Ogawa, M. Anpo, *Catal. Lett.* **2002**, *80*, 3.
[162] K. Soga, Y. Sano, T. Uozumi, Patent No. JP 2000063387, **2000**.
[163] M. Furuya, S. Riku, Patent No. JP 2002069015, **2002**.
[164] X. Gao, I. E. Wachs, MS Wong, J. Y. Ying, *J. Catal.* **2001**, *203*, 18.
[165] M. M. Yusuf, H. Imai, H. Hirashima, *J. Sol-Gel Sci. Technol.* **2002**, *25*, 65.
[166] Y. Takahara, J. N. Kondo, T. Takata, D. Lu, K. Domen, *Chem. Mater.* **2001**, *13*, 1194.
[167] V. F. Stone Jr., R. J. Davis, *Chem. Mater.* **1998**, *10*, 1468.
[168] N. Perkas, Y. Wang, Y. Koltypin, A. Gedanken, S. Chandrasekaran, *Chem. Commun.* **2001**, *11*, 988.
[169] H. Yoshitake T. Tatsumi, *Chem. Mater.* **2003**, *15*, 1695.
[170] X. He, D. Antonelli, *Angew. Chem. Int. Ed.* **2002**, *41*, 214.
[171] R. C. Schroden, C. F. Blanford, B. J. Melde, B. J. S. Johnson, A. Stein, *Chem. Mater.* **2001**, *13*, 1074.
[172] B. J. S. Johnson, A. Stein, *Inorg. Chem.* **2001**, *40*, 801.
[173] M. A. Carreon, PhD Thesis, University of Cincinnati, **2003**.
[174] A. Sayari, P. Liu, J. S. Reddy, *Mater. Res. Soc. Symp. Proc.* **1996**, *431*, 101.
[175] K. M. McGrath, D. M. Dabbs, N. Yao, K. J. Edler, I. A. Aksay, S. M. Gruner, *Langmui r* **2000**, *16*, 398.
[176] A. S. Malik, D. M. Dabbs, I. A. Aksay, H. E. Katz, *Mater. Res. Soc. Symp. Proc.* **2001**, 658.

Received August 3, 2004

